$$= \boldsymbol{V}_1^T \boldsymbol{J}^T(\boldsymbol{q}_d)(\boldsymbol{I} + \boldsymbol{G}_f)\delta\boldsymbol{\lambda} \quad (37)$$

$$\boldsymbol{V}_2^T \boldsymbol{M}(\boldsymbol{q}_d)\boldsymbol{V}_2 \delta\ddot{\boldsymbol{x}}_2 + \boldsymbol{V}_2^T \boldsymbol{C}\boldsymbol{V}_2 \delta\dot{\boldsymbol{x}}_2 + \boldsymbol{V}_2^T \boldsymbol{K}(\boldsymbol{q}_d, \boldsymbol{\lambda}_d)\boldsymbol{V}_2 \delta\boldsymbol{x}_2 = 0 \quad (38)$$

$$\delta\boldsymbol{x}_1 = 0. \quad (39)$$

From this decomposition, we see that the poles of the linearized differential-algebraic equations (19), (20) are actually the poles of the second order linear differential equation (38). This justifies the procedure for pole assignment given in the text.

REFERENCES

[1] S. Arimoto and F. Miyazaki, "Asymptotic stability of feedback control laws for robot manipulators," in *Proc. IFAC Symp. Robot Contr.*, Barcelona, Spain, 1985.

[2] R. K. Kankaanranta and H. N. Koivo, "Stability analysis of position-force control using linearized Cartesian space model," in *Proc. IFAC, Symp. Robot Control*, Karlsruhe, Germany, Oct. 5–7, 1988, pp. 95.1–95.6.

[3] T. Yoshikawa, "Dynamics hybrid position/force control of robot manipulators-description of hand constraints and calculation of joint driving forces," in *Proc. IEEE Conf. Robotics Automat.*, San Francisco, CA, 1986, pp. 1393–1398.

[4] N. H. McClamroch, "Singular systems of differential equations as dynamic models for constrained robot systems," in *Proc. IEEE Conf. Robotics Automat.*, Apr. 1986, San Francisco, CA.

[5] N. H. McClamroch and D. Wang, "Feedback stabilization and tracking of constrained robots," *IEEE Trans. Automat. Contr.*, vol. 33, pp. 419–426, May 1988.

[6] N. H. McClamroch, "Feedback stabilization of control systems described by a class of nonlinear differential-algebraic equations," *Syst. Contr. Lett.*, pp. 53–60, vol. 15, 1990.

[7] N. H. McClamroch and D. Wang, "Linear feedback control of position and contact force for a nonlinear constrained mechanism," *J. Dyn. Syst., Measurement Contr., ASME*, vol. 112, no. 4, pp. 640–645, Dec. 1990.

[8] J. K. Mills and A. A. Goldenberg, "Force and position control of manipulators during constrained motion tasks," *IEEE Trans. Robotics Automat.*, vol. 5, pp. 30–46, Feb. 1989.

[9] M. H. Raibert and J. J. Craig, "Hybrid position/force control of manipulators," *ASME J. Dyn. Syst., Measurement, Contr.*. vol. 102, pp. 126–133, June 1981.

[10] M. Takegaki and S. Arimoto, "A new feedback method for dynamic control of manipulators," *J. Dyn. Syst., Measurement Contr.*, vol. 102, pp. 119–125, 1981.

[11] D. Wang "Stability analysis and position/force control design for mechanical systems with holonomic constraints," Ph.D dissertation, 1989, Dept. Elec. Eng. Comput. Sci., The Univ. Michigan, Ann Arbor, MI.

[12] D. E. Whitney, "Force feedback control of manipulator fine motions," in *Proc. 1976 Joint Automat. Contr. Conf.*, pp. 687–693.

[13] O. Khatib, "A unified approach for motion and force control of robot manipulators: The operational space formulation," *IEEE J. Robotics Automat.*, vol. RA-3, pp. 43–53, 1987.

[14] X. Yun, "Dynamic state feedback control of constrained robot manipulators," in *Proc. 27th Conf. Decision Contr.*, Austin, TX, Dec. 1988, pp. 622–626.

[15] J. T. Wen and S. Murphy "Stability analysis of position and force control for robot arms," *IEEE Trans. Automat. Contr.*, vol. 36, pp. 365–371, Mar. 1991.

[16] M. Vidyasagar, *Nonlinear Systems Analysis*. Englewood Cliffs, NJ: Prentice-Hall, 1978.

Thermal Tactile Sensing

G. J. Monkman and P. M. Taylor

***Abstract*— The measurement of temperature change as an indication of a materials relative thermal conductivity has often been utilized as a means of tactile sensing. Unfortunately, the long time response of most thermal sensors makes such a technique too slow for normal industrial robotic uses. This paper considers the human tactile performance with particular regard to temperature sensing and introduces a new means by which a usable rise time may be achieved. Two methods, using devices hitherto not utilized for tactile sensing, are demonstrated.**

I. INTRODUCTION

According to Harmon [1] the requirement for a tactile sensor to emulate the human finger is a dynamic pressure range of three orders of magnitude with a resolution of 20 by 20 tactels per finger. A spatial resolution of better than 2 mm and a time response within 10 mS with low hysteresis are also desirable. Such a time response may be a little optimistic, even in the case of a physical displacement transducer this represents a displacement velocity of 0.1 m/s for a 1 mm depression. Though perhaps conservative for most robot transitions, this type of velocity is not very representitive of fine grasping actions where much slower movements are more usual.

As one may observe when touching objects with the finger tips, temperature is also an integral part of the human overall tactile sensing strategy. Thermal effects also help determine the "feel" or texture of a surface.

II. THE HUMAN TACTILE SENSE

We cannot consider the finger tips as tactile sensors in isolation without due regard to the human entity as a whole. As pointed out by Lederman [2]: in everyday life our fingers explore their environment, actively pushing against objects to determine their form. Unlike many inanimate compliant membranes, the very nature of flesh allows it to return completely to its original profile after depression very rapidly. Constant blood flow, and other physical movements, help to augment this positive recovery effect.

Much confusion is caused by the surface texture and the relative thermal conductivity of the material in question. Whenever such a sample is encountered, the finger is moved over the surface to give a feel for its surface profile, material stiffness, temperature etc. Furthermore, the human fingers contain at least five different receptor types, many of which are connected in a one-to-many configuration [3]. This must inevitably result in a high degree of cross-talk.

In a simple test, one may observe the inability of the human tactile sense to determine even relative temperatures by touching a selection of objects and then measuring their actual temperature with an accurate thermometer or thermocouple probe. This type of effect will be familiar to most children who have dipped a finger into bowls of water of varying temperature in an attempt to estimate their relative temperatures.

What our fingers detect thermally is not the absolute temperature of a material alone, but also its thermal conductivity and diffusivity.

Manuscript received April 2, 1991; revised May 28, 1992.

G. J. Monkman is with Fachhochschule Regensburg, Fachbereich Elektronik, Seyboth Straße, 8400 Regensburg, Germany.

P. M. Taylor is with the Robotics Research Unit, University of Hull, Hull, HU6 7RX. United Kingdom.

IEEE Log Number 9208254.

This is because the human finger is a source of heat, which at approximately 34°C is slightly above the ambient temperature of most objects we encounter. What the nerves in the finger detect is the outflow of heat from this source. This suggests that the human temperature sense may be emulated by thermal conduction sensing.

III. Thermal Sensing

In the same way that piezoelectric materials exhibit an electrical output when subjected to a mechanical stress or pressure, so do pyroelectric materials when heated or cooled. In fact the polyvinylidene flouride used by Dario [4] for piezoelectric tactile sensors also exhibits a pyroelectric effect [5].

Most thermal devices for tactile interrogation are active. They consist of both a heat source and sensor rather than attempting to measure absolute temperature by means of the sensor alone. Russell [6] demonstrates a 10 by 10 array of tactels using integral heating elements and thermistors. An extension to this is the 4 by 4 thermal array superimposed on an 8 by 8 capacitive array of force sensors shown by Siegel and co-workers [7].

In both the above cases some degree of material recognition is possible due to the different thermal conductivity characteristics of dissimilar materials. Unfortunately, in both cases temporal response was found to be very slow for the thermal sensors. A 90% rise and decay time of roughly 18 s was experienced by Siegel, whereas Russell appears to have achieved a 4-s rise time but again a decay of around 20 s. Two devices that yield superior performance in this respect are now described.

A. Peltier Device Sensors

For any thermal tactile sensor to be effective over a wide range of subject materials, it must be thermally active. That is to say, it must provide a positive temperature reference that is always above or below any subject temperature it is likely to encounter. Otherwise, materials existing at the same temperature as the sensor will not be detected. When an active thermal sensor is used, highly thermally insulating materials reflect the heat back toward the sensor. This results in an increase, rather than a decrease, in the energy absorbed by the sensor that not only provides an acknowledgement of tactile contact but also information allowing the material to be distinguished from other, thermally conducting or insulating materials.

The use of a small Peltier heat pump [8] allows the construction of a much faster-acting thermal sensor. The temperature differential between the hot and cold sides of the device is proportional to the drive current demand. Any externally caused change in this temperature differential, i.e. by dissipation of a quantity of the heat load into a thermally conductive medium, will result in a corresponding change in drive current. Experiments on a range of materials yield exponential rise and decay response curves. Fig. 1 shows typical response curves for a selection of three materials with different thermal conduction properties.

For a device with a 2 by 3 mm contact area [9], a typical dynamic range of between 0.05 and 0.1 Amps change in a mean drive current of 0.25 Amps was observed for the range of materials shown in Figs. 1 and 2.

By observing the curves of Fig. 1, the 63% rise time constant $\tau = 0.8$ s, and according to Fig. 2, the decay time constant $\tau_d = 3.4$ s.

The curves are of the form

$$I_o = \frac{V}{R} + I(1 - e^{-k_1 t}) \tag{1}$$

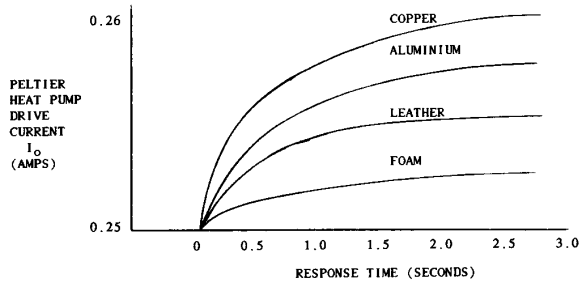

Fig. 1. Peltier heat pump rise time curves.

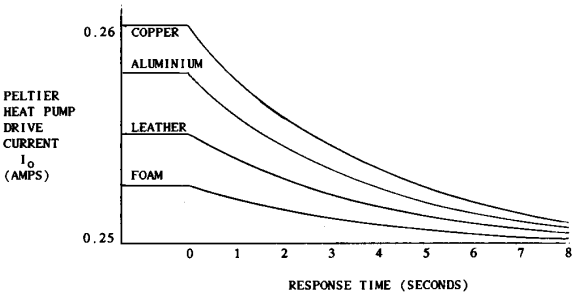

Fig. 2. Peltier heat pump decay time curves.

for the rise time, where $k_1 = 1/\tau_r$ and for the decay time

$$Io = \frac{V}{R} + Ie^{-k_2 t} \tag{2}$$

where $k_2 = 1/\tau_d$

In both cases V/R is the component due to resistive heating and may be taken as a constant.

Combining into (1) and (2) gives the characteristic:

$$I_o = \frac{V}{R} + (1 - \delta)I(1 - e^{-1.25t}) + \delta Ie^{-0.29t} \tag{3}$$

where $\delta = 0$ for thermal contact and $\delta = 1$ for release.

From {3} the rise time can be seen to be much faster than the decay time. For comparison with similar parameters often quoted in the literature, the 90% rise time is reasonably fast at approximately 1.8 s. Unfortunately, the 90% decay time of 7.8 s continues to present a problem. However, this is still faster than present "state of the art" thermal tactile sensors, which as mentioned in the beginning of Section III may have response times as long as 20 s.

The time constants also appear to be the same regardless of the subject material in which the device is in contact. Only the final steady state amplitude is representitive of the energy dissipation into the subject material due to heat transfer. This suggests that the time constants τ_r and τ_d are determined completely by the construction of the Peltier device in question, both in terms of dimensions and material properties. Naturally, the absolute temperature of a subject will affect the final amplitude as more energy will be dissipated in a cooler subject.

Naturally, due to the diffusivity of the material the sensor is in contact with, its physical thickness will have some influence on the final steady state value of the current flow. The diffusivity of a material is a function of its thermal conductivity, density and specific heat. It is a second-order effect that results when the heat flow into a material encounters a variable temperature gradient. This gradient may exist in more than one axis depending on the objects geometry [10]. This effect made itself most apparent when results between

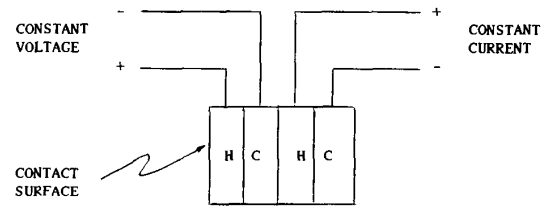

Fig. 3. Active heat sink configuration.

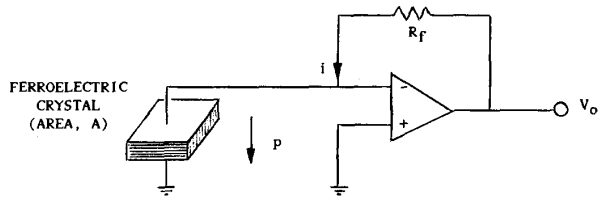

Fig. 4. Basic infrared detector circuit.

tests on aluminium foil (20 μ thick) and solid aluminium block were compared. For the aluminium foil, this resulted in a lowering of the final steady state output amplitude by approximately 15% compared to that obtained with the solid aluminium block. Similar results were obtained for copper foil compared to solid copper block.

The addition of a heat sink to the cold side of the Peltier device gave a slight quickening in rise time but with an attendant increase in the corresponding recovery time. With the addition of an active heat sink in the form of a second Peltier heat pump, driven by a constant current as shown in Fig. 3, the reduction and increase in rise and decay times respectively was found to be around 10%. Adding a further heat sink to the cold side of the second Peltier device did not appear to give any discernible change in overall response times.

Given that the time constants are wholly dependant on the physical construction of the Peltier heat pump, much smaller devices are likely to exhibit faster response times. This gives great potential to the fabrication of such sensors in arrays using VLSI technology to which Peltier devices, being basically semiconductors, are ideally suited. By detecting changes in thermal effects rather than by trying to measure absolute values offers the promise of much faster response times.

B. Pyrometers

Very few semiconductor materials perform well in the far infrared. Mercury/Cadmium Telluride (Hg/Cd Te) and Lead/Tin Telluride (Pb/Sn Te) are active between 8 and 14 μm but require an operating temperature of 77 K and are therfore usually restricted to sophisticated military applications [11]. More practical are ferro-electric crystals that are capable of very fast responses, so much so that they can be used to detect infrared signals modulated at several MHz. A typical arrangement is shown in Fig. 4 [12].

Analysis of this circuit gives

$$V_o = R_f i = R_f A_p \frac{\partial T}{\partial t} \tag{4}$$

where p is the pyroelectric coefficient (C m^{-2} K^{-1}), dependant on the dielectric properties and specific heat of the crystal element [13]. The factor R_v is the responsivity of the crystal material and depends on both the thermal response to incident radiation and the pyroelectric response to the temperature change ΔT to incident radiation of power $W(t)$.

$$c\frac{dT}{dt} + G\Delta T = eW(t) \tag{5}$$

where c is the heat capacity of the crystal (JK^{-1}), G is thermal conductance (Js^{-1} K^{-1}) and e is the fraction of effective incident power thermalising the crystal.

The voltage responsivity R_v in volts/watt of incident radiation is given in (6), where R is the electrical input resistance.

$$\textit{Voltage responsivity } R_v = \frac{A_e R_p}{c}. \tag{6}$$

Burfoot and Taylor [13] (among others) provide tables of values of R_v and other parameters for the selection of suitable materials. In most cases thermal relaxation time restricts the frequency response to the range 1 to 100 Hz [12]. Bandwidth of the detector can be increased by decreasing the input resistance R, but as can be seen from (6) this will result in a corresponding loss of responsivity.

Rearranging (6) gives

$$p = \frac{R_v c}{AeR}. \tag{7}$$

Combining (4) and (7) produces an expression (8) for the output voltage.

$$V_0 = \frac{R_f}{R}\frac{R_v c}{e}\frac{dT}{dt}. \tag{8}$$

From (8) it can be seen that improving the responsivity will increase the output voltage V_0 but, as mentioned previously, at the cost of a reduction in operating bandwidth. A more practical means of raising the output voltage is by increasing the gain factor R_f/R within the usual gain bandwidth product and noise constraints of the chosen operational amplifier.

What is important about (4) is the influence of $\partial T/\partial t$ on the output voltage V_0. This shows that only a change in temperature will produce a resultant output V_0. The limiting factor with regard to response time is due to the crystal resistance and capacitance together with that of the housing (which is usually dominant). As most commercially available devices are only available in hermetically sealed enclosures (often because of the deliquescent nature of many ferroelectric crystal materials), there is little the end user can do to improve the behaviour. However, during fabrication of large arrays some steps may be taken to optimise on the desired parameters, in this case response time.

The upper limit on operating temperature for most ferroelectric materials is in the region of 60°C. This may pose a problem in a few robotic applications where relatively high temperatures are involved, though this is likely to be a minority of cases.

Such devices are commonly available in the form of pyrometers of the type used in Infrared security detector systems. The sensor elements have a typical radiation detection frequency range of 5 to 15 μm [14]. Being electrically polarized, usually 2 complimentarily connected elements are included in each pyrometer package. This accounts for the opposite polarity in the contact and removal response curves of Fig. 6. Unfortunately, these are essentially passive devices that provide no heat source of their own. Consequently an additional heat source, for example a simple resistive heating element, must be provided. Fig. 5 shows a typical construction of such a thermal tactile sensing device. Though the actual elements are very small (approximately 2 mm square) they are normally housed in a TO39, or in this case, a 6-pin DIL package about 7 mm square.

In the aforementioned experimental device, the heating element consists of a simple electrically resistive element etched on to a layer of PCB foil, driven by a current of approximately 2 amps. The thermally conductive layer comprises of an opaque film to elliminate effects of electromagnetic IR radiation whilst at the same time allowing heat to be transferred though the film and radiated on to the sensing elements. It is necessary for this film to be as thin as possible so as not to act as a heat sink thereby reducing the

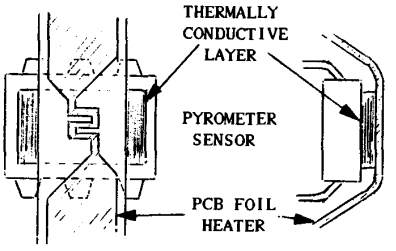

Fig. 5. Pyrometer tactel.

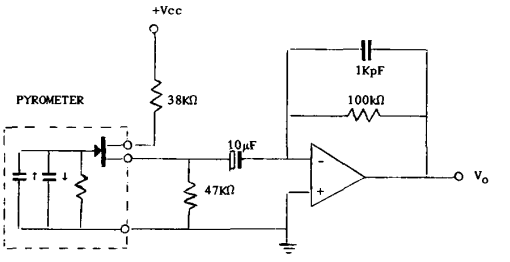

Fig. 7. Pyrometer amplifier circuit.

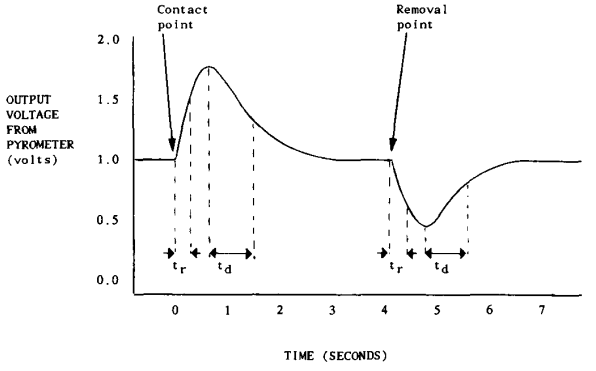

Fig. 6. Pyrometer response curves.

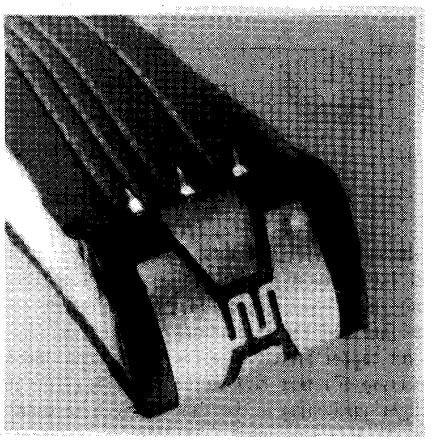

Fig. 8. Combined thermal, electrical and mechanical tactile sensor.

response time. A thin layer of aluminium foil sufficed but conductive aluminium paint was found to give a slight improvement in response time over that of the aluminium foil.

Fig. 6 shows a typical response curve for contact and release from a thermally conducting subject, as would be observed from the output of an amplifier such as that in Fig. 4 or 7. As can clearly be seen from these plots, both the rise and decay times are relatively fast. This is particularly apparent in the 63% rise time of approximately 260 mS (600 mS for a 90% rise time) for the response caused by initial contact. The recovery and return to the original state is somewhat slower at 800 mS (1.8 s for 90%). However, with the sensor elements being basically capacitive in nature, these sensors only detect temperature change and cannot measure absolute temperature levels. This is of course very similar to the human tactile model. The second pulse in Fig. 6, of opposite polarity, represents the effects of subject removal and has a similar time response to the contact curve. When used with thermally insulating subjects, the pulses are in the reverse direction, due to the measured energy being increased.

A suitable amplifier circuit, designed to obtain a usable sensitivity and a good frequency response from the pyrometer sensor, is shown in Fig. 7. The design criteria is not strict and may be adapted to suite the intended use.

Using the pyrometer tactel construction of Fig. 5 on four different material subjects, together with the amplifier arrangement of Fig. 7, continuous testing yielded the statistical results shown in Table I.

Though the accuracy of the figures shown in Table I is not high enough for precise measurement purposes, discrimination between material types is good enough for positive identification within this set of samples. As the main measurand is thermal conductivity this parameter will be the limiting factor in any attempt to differentiate between two materials using this technique. The thermal conductivity of copper being typically 60% higher than that of aluminium alloy suggests that the difference in output voltage amplitudes for the two

TABLE I
PEAK AMPLITUDES FOR FOUR MATERIAL SUBJECTS

Material Type	Average Peak Amplitude (mV)	Standard Deviation	SD AS % of Average
Copper	1062	144.6	13.6
Aluminum	750	94.6	12.6
Leather	431	64.3	14.9
Foam	−186	37.0	19.8

metals shown in Table I is of the expected order. The negative sign in front of the amplitude for the polyester foam sample is due to the thermal conductivity being effectively negative in that heat is reflected rather than absorbed. The larger standard deviation associated with the tests on this sample is almost certainly due to the very uneven surface texture and the unpredictable nature of its physical compliance.

One of the main advantages of this kind of device, like the Peltier heat pump, is its ability to be fabricated into arrays in VLSI form. The only potential problem is the foil heaters used in the experimental model of Figs. 5 and 8. If used in an array these could not be wired in series due to the variation in line current caused by changes in electrical resistance when one or more elements of the same line are brought into contact with a cooler medium. So unless higher voltage, lower current heaters could be utilized, arranging all elements of an 8 by 8 array of foil heater elements in parallel would require a supply current of 128 amps!

In an integrated construction, a more robust method would be to replace the heating element with a very small Peltier device, in parallel with a zener diode to maintain voltage stability. These may then be conected in series/parallel combinations allowing a more realistic supply scheme to be employed.

Ferroelectric devices can also be electrically modulated to produce a time varying thermal emission [13]. It is conceiveable that such an alternating heat source in conjunction with a similar detector device could enable continuous measurements of thermal conduction to be made.

Given a fast enough response time of the thermal emitter, it is possible to pulse the emitter and observe changes in the reflected thermal energy. This would naturally be greater when the device is in contact with a thermally insulating, rather than conducting subject. Though the simple heating elements used in the prototype of Fig. 5 is likely to be too slow, a ferroelectric emitter, or even a heating element of the kind used in dye diffusion thermal colour printing heads would be quick enough. Such heating elements are deposited as linear arrays using thin film processes and are capable of rise times of around 10 mS [15].

IV. Combination with Electrical Resistance and Force Sensing Tactels

Slight changes in thermal conductivity can be measured in many materials, including water, between 200 and 400° K, particularly at the solid/liquid transition point [16]. This is not however usually found with most metals above 100° K. This coupled with differences of thermal conduction in samples of the same material due to differences in texture, mass etc suggests that measuring thermal properties in isolation can only provide an indication of an unknown samples composition. For example, though the standard deviations for the statistical tests of Table I are narrow enough for discrimination between most metals, materials with very similar thermal conductivities such as molybdenum and silicon are likely to prove more difficult. For these reasons thermal tactile sensors are likely to be of more use when combined with other sensors.

Like the anthropormorphic model, combinations of several tactile sensors has been investigated. Siegel combined both thermal and mechanical sensors [7]. Unfortunately, as mentioned previously, the thermal sensor had a much poorer response than the mechanical tactile device. Fig. 8 shows a combined thermal and mechanical device with the addition of an electrical resistance sensor. This allows a subjects electrical conductivity to be ascertained (something the human tactile sensor cannot do). The thermal sensor being a pyrometer and heater, of the type depicted in Fig. 4, the response is comparatively fast.

The electrical resistance measurement is provided by additional sensor tracks etched onto the same PCB foil as the heater element. This allows the sensor to distinguish between electrical and thermal conduction properties. There are valid reasons for this. Carbon fibre is a good electrical conductor, though a relatively poor thermal conductor. Conversely, materials like mica, used as electrical barriers between high power dissipation electronic components and heat sinks, are extremely poor electrical, but good thermal conductors. Many pressure sensitive devices are commercially available, some of which are fabricated as flexible films such as force sensing resistors [17] mentioned previously. These may be incorporated at a convenient position beneath the thermal sensor.

Very few tactile sensors are commercially available and those that are usually comprise of arrays of elements whose electrical resistance decreases with increasing applied mechanical force. One such device that does not appear to suffer from the problems of severe hysteresis and poor longevity, traditionally associated with mechanical tactile sensors, is the FSR^{TM} (force sensing resistor) made by *Interlink* [17]. Such devices exhibit less than 2 mS response times and are almost totally imune to temperature variations. Being thus limited to one measurand only makes them ideally suited to combining with other tactile sensors without fear of cross-talk.

When solid objects are encountered, the displacement of the FSR tactel is extremely small hence the electrical resistance change experienced is proportional to the applied force. Therefore the measurand may be considered to be stress rather than strain. On the other hand, when the tactel comes into contact with soft or compliant surfaces, considerable displacement is possible from the initial contact point revealed by the thermal and/or resistive sensors. This displacement, measured by the robots position encoders, represents the strain undergone by the object. In conjunction with the force measurement from the FSR it can be used to calculate the elastic modulus of the object material.

$$\text{Elastic modulus, } E = \frac{\text{stress}}{\text{strain}} = \frac{\sigma}{\epsilon}. \tag{9}$$

where

$$\text{stress, } \sigma = \text{force/area} \tag{10}$$

and, the elastic displacement from an initial state ℓ_o to a final state ℓ gives the true strain ϵ :

$$\epsilon = \int_{\ell_0}^{\ell} \frac{d\ell}{\ell} = \ln\left(\frac{\ell}{\ell_o}\right). \tag{11}$$

The actual area of contact may be assumed constant for a small tactel element so that the final measurand may either be stress, strain or elastic modulus depending of whether the tactel is in contact with a rigid or non-rigid surface.

With all three sensing techniques combined, a very powerfull tool for the identification of material types becomes available. However, there will always be materials with such similar characteristics in all respects as to make them virtually indistinguishable. For example copper and silver have very close thermal and electrical conductivities whilst both being rigid solids. Humans usually distinguish between the two by a number of methods including the use of vision, apriori information etc. However, even the intelligent combination of all the human senses have often been fooled since before the time of Archimedes!

V. Conclusion

This paper has considered the human tactile model together with its failings when used to measure any single parameter independantly of others that may also be present. The necessity of employing simultaneously, yet independantly operating sensor elements has been stressed.

Two new thermal tactile methods have been demonstrated and evaluated in comparison to other forms of thermal tactile sensing which have previously been tried. This has led to an improvement in response time of roughly one order of magnitude over previous devices.

One of the new thermal techniques has been combined with two other tactile sensing methods to provide a three parameter tactel. Unlike the human model, each measurand can be ascertained independantly with this combination.

Combined with other semiconductor sensors, and in the light of current VLSI fabrication technology, the manufacture of tactile arrays using these techniques should prove considerably easier than with many of the mechanical tactile methods used in the past.

References

[1] L. D. Harmon, "Automated tactile sensing," *Int. J. Robotics Res.*, vol 1, no. 2, pp. 3–32, 1982.

[2] S. Lederman, "Human haptics,"*Office of Naval Research Workshop on Dextrous Manipulation and Teleoperation*, Univ. Oxford, Aug. 1989.

[3] J. S. Albus, "Brains, behaviour and robotics," *BYTE*, pp. 39–40, 1981.

[4] P. Dario, C. Domenici, R. Bardelli, D. De Rossi, and P. C. Pinotti, "Piezoelectric polymers: New sensor materials for robotic applications," in *Proc. 13th Int. Symp. Ind. Robots*, Chicago, Apr. 1983, pp. 14.34–14.49.
[5] G. Caldwell, "Novel sensor and gripper design," B.Sc. thesis, Univ. Hull, Hull, UK, 1986.
[6] R. A. Russell, "Thermal sensor for object shape and material constitution," *Robotica*, vol. 6, pp. 31–34, Mar. 1988.
[7] D. Siegel, I. Garabieta, and J. M. Hollerbach, "An integrated tactile and thermal sensor," in *Proc. IEEE Int. Conf. Robotics Automat.*, 1986.
[8] E. A. Desloge, *Thermal Physics*. New York: Holt, Rinehart, and Winston, 1968.
[9] "Thermoelectric cooler installation Guide," Marlow Industries, Dallas, TX, 1989.
[10] D. Elwell and A. J. Pointon, *Classical Thermodynamics*, Harmondsworth, Middlesex, UK: Penguin, 1972, pp. 275–277.
[11] A. Bar-Lev, *Semiconductors and Electronic Devices*. Englewood Cliffs, NJ: Prentice Hall, 1979, pp. 141–142.
[12] M. E. Lines and A. M. Glass, *Principles and Applications of Ferroelectrics and Related Materials*. Oxford, UK: Clarendon, 1977, pp. 141–144 and 561–563.
[13] J. C. Burfoot and G. W. Taylor, *Polar Dielectrics and Their Applications*. New York: MacMillan, 1979, pp. 381–384.
[14] RS Components Ltd., "Pyroelectric detector kit," *RS Data Library 10906*, Nov. 1990.
[15] P. W. Webb and R. A. Hann, "Measurement of thermal transients in a thermal print head used for dye diffusion colour printing," *IEE Proc. A; Sci., Measurement, Technol.*, vol. 138, no. 1, Jan. 1991, pp. 98–100.
[16] M. W. Zemansky, *Heat and Thermodynamics*. New York: McGraw Hill, 1957, pp. 84–86.
[17] Interlink, *Force and Position Sensing Resistors: An Emerging Technology*, Technical Overview Rev. 2/90, Interlink Electronics, Luxembourg, 1990.

Dynamic Calibration and Compensation of a 3-D Laser Radar Scanning System

Y. D. Chen and J. Ni

Abstract—**LIDAR (laser radar) is used to measure three-dimensional (3-D) object positions. It produces a range and an intensity image of the measured object and relies on the range image to determine the 3-D positions of the object. But, the range image is frequently corrupted with noise. A dynamic calibration method has been established to improve the LIDAR accuracy based on a polynomial calibration model and an autoregressive moving average (ARV) calibration model. Experimental results show that the measurement errors of the LIDAR system have been reduced from 163 counts to 18 counts after compensation using the polynomial calibration model and that the errors have been further reduced to 11 counts with the ARV model.**

I. Introduction

In many applications it is necessary to determine the 3-dimensional positions of an object. LIDAR, as a 3-D active range sensor, has been used in applications such as bin picking, robotic assembly, postal package recognition, etc. In order to report the object positions in the world coordinates, the system is calibrated. That is, the 3-D camera location is estimated. If the camera location is known in the world coordinates, the object position sensed in the field of view of the camera can be transformed to the world coordinates.

For the camera location problem, early work was done by several researchers. Liu and Huang [9] used 3-D line or point correspondences to compute the rotation matrix and translation vector. Fischler and Bolles [3] found the solution by computing the lengths of rays from the focal points of a camera to several "control points" in the image plane. This algorithm is nonlinear and usually six point correspondences are required to get a unique solution.

In the early work of the camera location problem, only intensity images were used, and the quantization errors and measurement noises were smoothed out during the estimation procedures. Furthermore, no error compensation algorithms for images have been investigated.

In contrast to conventional vision sensors, LIDAR sensors can produce two images, range and intensity, at the same time. By scanning the LIDAR beam in a point-by-point fashion over an object in the field of view of the LIDAR, a map of range and intensity images of the 3-D object can be obtained. The beam location at each sampling instance will be considered as the pixel location of the image. The range image at each pixel represents the distance measured from the sensor to the object at the sensor coordinates, and the intensity image is the measurement of the reflection of the object at the same pixel as the range image.

However, experimental results show that the LIDAR range image is usually corrupted severely by noise and it must be compensated for before it can be used accurately in real applications. The results also indicate that its intensity image is very robust due to the unique intensity image generation mechanism of the LIDAR sensor.

This paper describes a novel method to dynamically calibrate the LIDAR system. The method compensates for the range image errors by identifying a dynamic model between the range image errors and the intensity images. In the following sections, the principles of the LIDAR sensor and a LIDAR scanning system will be introduced. The calibration procedures will be described and a new method to compensate for range images will be proposed and tested.

II. Principles of the LIDAR Sensor and Scanning System

LIDAR range image sensors collect large amount of three dimensional coordinate data from visible surfaces of an object. They are unique image devices in that the image data points explicitly represent the scene surface geometry in a sampled form.

There are two types of LIDAR scanners: (1) coherent (FM) LIDAR—which incorporates frequency modulation and mixing, and (2) phase shift (AM) LIDAR—which correlates the phase shift between outgoing and incoming amplitude modulated light beams. The LIDAR used in this paper is an AM LIDAR. It scans an object in a point-by-point fashion, and its hardware structure allows high-speed data sampling.

Fig. 1 illustrates some fundamental aspects of AM LIDAR, and Fig. 2 is a schematic diagram of the LIDAR scanner. Fig. 1(a) shows how the modulated laser beam is projected out of the scanner head toward the surface of an object. The diffused reflection of the beam off the surface is received by a detector telescope. The outgoing and incoming beams use different optical elements by including a small parallax angle between the optical axes (typically less than 0.5°), thus reducing the effects of light scatter and crosstalk.

Fig. 1(b) shows how phase shift ranging is performed by comparing the relative offset of the zero crossings of the outgoing and incoming

Manuscript received September 23, 1991.
Y. D. Chen is with Perceptron, Inc., 23855 Research Drive, Farmington Hills, MI 48024.
J. Ni is with the Department of Mechanical, Engineering and Applied Mechanics, The University of Michigan, Ann Arbor, MI 48109.
IEEE Log Number 9207369.